Journal of Applied Fluid Mechanics, Vol. 9, No. 5, pp. 2457-2467, 2016.
Available online at www.jafmonline.net, ISSN 1735-3572, EISSN 1735-3645.

Transient MHD Free Convection Flow and Heat Transfer of Nanofluid past an Impulsively Started Semi-Infinite Vertical Plate

V. Rajesh[1†], A. J. Chamkha[2] and M. P. Mallesh[1]

[1] *Department of Engineering Mathematics, GITAM University Hyderabad Campus, Rudraram, Patancheru Mandal, Medak Dist.-502 329, Telangana. India.*
[2] *Mechanical Engineering Department, Prince Mohammad Bin Fahd University (PMU) Al-Khobar, Kingdom of Saudi Arabia*

†*Corresponding Author Email: v.rajesh.30@gmail.com*

(Received June 19, 2014; accepted December 28, 2015)

ABSTRACT

In this paper, the problem of nanofluid flow and heat transfer due to the impulsive motion of a semi-infinite vertical plate in its own plane in the presence of magnetic field is analyzed by the implicit finite-difference numerical method. A range of nanofluids containing nanoparticles of aluminium oxide, copper, titanium oxide and silver with nanoparticle volume fraction range less than or equal to 0.04 are considered. The Tiwari-Das nanofluid model is employed. The velocity and temperature profiles as well as the skin friction coefficient and Nusselt number are examined for different parameters such as nanoparticle volume fraction, nanofluid type, magnetic parameter and thermal Grashof number. The present simulations are relevant to magnetic nanomaterials thermal flow processing in the chemical and metallurgical industries.

Keywords: Free convection; Nanofluids; Implicit finite-difference numerical method; MHD; Semi-infinite vertical plate; transient flow; Materials processing.

1. INTRODUCTION

Transient free convection flows under the influence of a magnetic field have attracted the interest of many researchers in view of their applications in modern materials processing where magnetic fields are known to achieve excellent manipulation and control of electrically-conducting materials (Ibrahim and Shanker (2014)). Magnetohydrodynamic (MHD) convection flows also find significant applications in renewable energy devices including MHD power generators (Chen *et al*. (2005), Yamaguchi *et al*. (2011)) as well as nuclear reactor transport processes (Mukhopadhyay (2011)) wherein magnetic field is employed to regulate heat transfer rates. Several authors have studied the natural convection hydromagnetic boundary layer flow of an electrically-conducting fluid. Mention may be made of research studies of Beg *et al*. (2011), Das *et al*. (2014), Gangadhar (2015), Seth *et al*. (2015) and ELKabeir *et al*. (2015).

Conventional heat transfer fluids, for example oil, water, and ethylene glycol mixtures, are poor heat transfer fluids because of their poor thermal conductivity. Application of these fluids as a cooling tool enhances manufacturing and operating costs. Many attempts have been taken by many researchers to enhance the thermal conductivity of these fluids by suspending nano/micro particles in liquids (Abu-Nada *et al*. (2012), Choi (1995)). Nanofluids are made of ultrafine nanoparticles (<100 nm) suspended in a base fluid, which can be water or an organic solvent (Choi (2009)). Nanofluids are found to exhibit higher conductive, minimum clogging, boiling, and convective heat transfer performances compared to conventional fluids (Akbarinia *et al*. (2011), Murshed *et al*. (2011), Yu *et al*. (2008)). There have been published several recent studies on the modelling of natural convection heat transfer in nanofluids: Daungthongsuk and Wongwises (2008) studied effect of the thermophysical properties models on the predicting of the convective heat transfer coefficient for low concentration nanofluid. Abu-Nada and Oztop (2009) presented the effects of inclination angle on natural convection in enclosures filled with Cu-water nanofluid. The Cheng-Minkowycz problem for natural convective boundary-layer flow in a porous medium saturated by a nanofluid was discussed by Nield and Kuznetsov (2009). The problem of mixed convection MHD flow of a nanofluid past a stretching permeable surface in the presence of Brownian motion and thermophoresis effects was studied by Chamkha *et al*. (2010a). Also, Chamkha

et al. (2010b) presented the non similar solution for natural convective boundary layer flow over a sphere embedded in a porous medium saturated with a nanofluid. Gorla *et al*. (2011a) studied Heat transfer in the boundary layer on a stretching circular cylinder in a nanofluid. Later, the problem of mixed convection past a vertical wedge embedded in a porous medium saturated by a nanofluid was analyzed by Gorla *et al*. (2011b). Free convection boundary layer flow of a non-Newtonian fluid over a permeable vertical cone embedded in a porous medium saturated with a nanofluid was discussed by Rashad *et al*. (2011). Chamkha *et al*. (2011) analyzed the unsteady boundary-layer flow of a nanofluid over a horizontal stretching plate in the presence of melting effect. Also, the problem of mixed convection boundary-layer flow over an isothermal vertical wedge embedded in a porous medium saturated with a nanofluid was studied by Chamkha *et al*. (2012). The problem of heat and mass transfer of unsteady natural convection flow of some nanofluids past a vertical infinite flat plate with radiation effect was studied by Turkyilmazoglu and Pop (2013). Loganathan *et al*. (2013) studied the effects of radiation on an unsteady natural convective flow of a nanofluid past an infinite vertical plate. Turkyilmazoglu (2014) analyzed the unsteady convection flow of some nanofluids past a moving vertical flat plate with heat transfer by the usual Laplace transform technique. Rajesh *et al*. (2014) presented the numerical study of Transient nanofluid flow and heat transfer from a moving vertical cylinder in the presence of thermal radiation. Later Rajesh and Anwar Beg (2014) studied MHD transient nanofluid flow and heat transfer from a moving vertical cylinder with temperature oscillation. Recently Rajesh *et al*. (2016) analyzed the Nanofluid flow past an impulsively started vertical plate with variable surface temperature. In all these recent studies (Turkyilmazoglu and Pop (2013), Loganathan *et al*. (2013), Turkyilmazoglu (2014), Rajesh *et al*. (2014), Rajesh and Anwar Beg (2014), Rajesh *et al*. (2016)), The Tiwari-Das (2007) nanofluid model is employed.

The aim of the present study is to examine the effects of the transverse magnetic field on a transient free convective flow of a nanofluid past an impulsively started semi-infinite vertical plate. The governing boundary layer equations along with the initial and boundary conditions are solved by an implicit finite difference method of the *Crank-Nicolson* type, which is unconditionally stable and convergent. Numerical results for the transient velocity and temperature profiles as well as the axial distributions of the skin-friction coefficient and local Nusselt numbers are presented and discussed in tables and graphs. The present study also provides an important benchmark for further simulations of magneto-nanofluid dynamic transport phenomena of relevance to materials processing, with alternative computational algorithms (e.g. Finite element methods).

2. MATHEMATICAL ANANLYSIS

We consider the unsteady, laminar, two-dimensional, boundary layer free convective flow of a viscous incompressible electrically conducting nanofluid past an impulsively started semi-infinite vertical plate in the presence of an applied magnetic field. The *x*-axis is taken along the plate in the vertical upward direction, and the y-axis is taken normal to the surface of the plate as shown in Figure 1.The gravitational acceleration g acts downward. Initially, both the plate and the nanofluid are stationary at the same temperature T'_∞ .They are maintained at this condition for all $t' \le 0$.

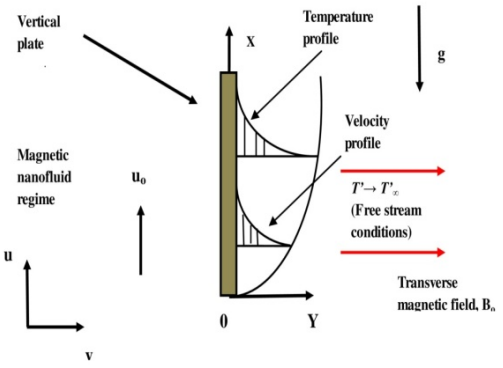

Fig. 1. The physical model and coordinate system.

At time $t' > 0$, the plate is given an impulsive motion in the vertically upward direction with the constant velocity u_0. The surface of the plate is maintained at a constant temperature T'_w higher than the temperature T'_∞ of the ambient nanofluid. We assume that the uniform magnetic field with an intensity of B_0 acts in the normal direction to the plate and the effect of the induced magnetic field is negligible, which is valid when the magnetic Reynolds number is small. The fluid considered is water-based nanofluid containing different types of nanoparticles: aluminium oxide (Al_2O_3), copper (Cu), titanium oxide (TiO_2) and silver (Ag). In this study, nanofluids are assumed to behave as single-phase fluids with local thermal equilibrium between the base fluid and the nanoparticles suspended in them so that no slip occurs between them. A schematic representation of the physical model and the coordinate system is depicted in Figure. 1. The thermo physical properties of the nanofluids are given in Table 1 (see Oztop and Abu-Nada (2008), Loganathan *et al*. (2013),). The boundary layer and Boussinesq approximations are assumed to be valid. Under these assumptions, the governing boundary layer equations according to the model for nanofluids given by Tiwari and Das (2007) can be written in dimensional form as

$$\frac{\partial u}{\partial x} + \frac{\partial v}{\partial y} = 0 \qquad (1)$$

Table 1 Thermo-physical properties of water and nanoparticles

	$\rho\left(Kg\,m^{-3}\right)$	$C_p\left(J\,Kg^{-1}K^{-1}\right)$	$\kappa\left(Wm^{-1}K^{-1}\right)$	$\beta\times10^{-5}\left(K^{-1}\right)$
H_2O	997.1	4179	0.613	21
Al_2O_3	3970	765	40	0.85
Cu	8933	385	401	1.67
TiO_2	4250	686.2	8.9528	0.9
Ag	10500	235	429	1.89

Table 2 Thermal conductivity and dynamic viscosity for various shapes of nanoparticles

Model	Shape of nanoparticles	Thermal conductivity	Dynamic viscosity
I	Spherical	$\frac{\kappa_{nf}}{\kappa_f}=\frac{\kappa_s+2\kappa_f-2\phi\left(\kappa_f-\kappa_s\right)}{\kappa_s+2\kappa_f+\phi\left(\kappa_f-\kappa_s\right)}$	$\mu_{nf}=\frac{\mu_f}{\left(1-\phi\right)^{2.5}}$
II	Spherical	$\frac{\kappa_{nf}}{\kappa_f}=\frac{\kappa_s+2\kappa_f-2\phi\left(\kappa_f-\kappa_s\right)}{\kappa_s+2\kappa_f+\phi\left(\kappa_f-\kappa_s\right)}$	$\mu_{nf}=\mu_f\left(1+7.3\phi+123\phi^2\right)$
III	Cylindrical (nanotubes)	$\frac{\kappa_{nf}}{\kappa_f}=\frac{\kappa_s+\frac{1}{2}\kappa_f-\frac{1}{2}\phi\left(\kappa_f-\kappa_s\right)}{\kappa_s+\frac{1}{2}\kappa_f+\phi\left(\kappa_f-\kappa_s\right)}$	$\mu_{nf}=\frac{\mu_f}{\left(1-\phi\right)^{2.5}}$
IV	Cylindrical (nanotubes)	$\frac{\kappa_{nf}}{\kappa_f}=\frac{\kappa_s+\frac{1}{2}\kappa_f-\frac{1}{2}\phi\left(\kappa_f-\kappa_s\right)}{\kappa_s+\frac{1}{2}\kappa_f+\phi\left(\kappa_f-\kappa_s\right)}$	$\mu_{nf}=\mu_f\left(1+7.3\phi+123\phi^2\right)$

$$\frac{\partial u}{\partial t'}+u\frac{\partial u}{\partial x}+v\frac{\partial u}{\partial y}=\frac{\mu_{nf}}{\rho_{nf}}\frac{\partial^2 u}{\partial y^2}+\frac{\left(\rho\beta\right)_{nf}}{\rho_{nf}}g\left(T'-T'_\infty\right)-\frac{\sigma B_0^2 u}{\rho_{nf}} \tag{2}$$

$$\frac{\partial T'}{\partial t'}+u\frac{\partial T'}{\partial x}+v\frac{\partial T'}{\partial y}=\frac{\kappa_{nf}}{\left(\rho C_p\right)_{nf}}\frac{\partial^2 T'}{\partial y^2} \tag{3}$$

The initial and boundary conditions for the problem are

$$\begin{aligned} &t'\le 0: u=0, v=0, T'=T'_\infty \text{ for all x and y}\\ &t'>0: u=u_0, \quad v=0, T'=T'_w \text{ at } y=0\\ &\qquad u=0, \quad T'=T'_\infty \text{ at } x=0\\ &\qquad u\to 0, \quad T'\to T'_\infty \text{ as } y\to\infty \end{aligned} \tag{4}$$

Here u is the velocity along x-axis; t' is the time; g is the acceleration due to gravity; T' is the temperature of the fluid; T'_∞ is the temperature of the fluid far away from the plate; T'_w is the temperature of the plate, ρ_{nf} is the effective density of the nanofluid, μ_{nf} is the effective dynamic viscosity of the nanofluid, β_{nf} is the thermal expansion of the nanofluid, κ_{nf} is the thermal conductivity of the nanofluid.

For nanofluids the expressions of density ρ_{nf}, thermal expansion coefficient $\left(\rho\beta\right)_{nf}$ and heat capacitance $\left(\rho C_p\right)_{nf}$ are given by

$$\begin{aligned} \rho_{nf}&=\left(1-\phi\right)\rho_f+\phi\rho_s\\ \left(\rho\beta\right)_{nf}&=\left(1-\phi\right)\left(\rho\beta\right)_f+\phi\left(\rho\beta\right)_s\\ \left(\rho C_p\right)_{nf}&=\left(1-\phi\right)\left(\rho C_p\right)_f+\phi\left(\rho C_p\right)_s \end{aligned} \tag{5}$$

The effective thermal conductivity of the nanofluid according to Hamilton and Crosser (1962) model is given by

$$\frac{\kappa_{eff}}{\kappa_f}=\frac{\kappa_s+\left(n-1\right)\kappa_f-\left(n-1\right)\phi\left(\kappa_f-\kappa_s\right)}{\kappa_s+\left(n-1\right)\kappa_f+\phi\left(\kappa_f-\kappa_s\right)} \tag{6}$$

Where "n" is the empirical shape factor for the nanoparticle. In particular $n=3$ for spherical shaped nanoparticles and $n=3/2$ for cylindrical ones. ϕ is the solid volume fraction of nanoparticles, μ is the dynamic viscosity, ν is the kinematic viscosity, β is the thermal expansion coefficient, ρ is the density and κ is the thermal conductivity. Here the subscripts nf, f and S represent the thermo physical properties of the nanofluids, base fluid and the solid nanoparticles, respectively.

The following dimensionless parameters are defined:

$$X = \frac{xu_0}{\nu_f} = \frac{x}{L_{ref}}, Y = \frac{yu_0}{\nu_f} = \frac{y}{L_{ref}}, t = \frac{t'u_0^2}{\nu_f},$$
$$U = \frac{u}{u_0}, V = \frac{v}{u_0}, G_r = \frac{g\beta_f \nu_f (T_w' - T_\infty')}{u_0^3},$$
$$P_r = \frac{\nu_f}{\alpha_f}, \; T = \frac{T' - T_\infty'}{T_w' - T_\infty'}, \; M = \frac{\sigma B_0^2 \nu_f}{\rho_f u_0^2} \tag{7}$$

With the non-dimensional variables (7), Equations (1)-(3) become

$$\frac{\partial U}{\partial X} + \frac{\partial V}{\partial Y} = 0 \tag{8}$$

$$\frac{\partial U}{\partial t} + U\frac{\partial U}{\partial X} + V\frac{\partial U}{\partial Y} = \frac{1}{\left(1-\phi+\phi\frac{\rho_s}{\rho_f}\right)}\left(\begin{array}{l}\frac{1}{(1-\phi)^{2.5}}\frac{\partial^2 U}{\partial Y^2} \\ +\left(1-\phi+\phi\frac{(\rho\beta)_s}{(\rho\beta)_f}\right)GrT \\ -MU\end{array}\right) \tag{9}$$

$$\frac{\partial T}{\partial t} + U\frac{\partial T}{\partial X} + V\frac{\partial T}{\partial Y} = \frac{1}{\left(1-\phi+\phi\frac{(\rho C_p)_s}{(\rho C_p)_f}\right)}\frac{\kappa_{nf}}{\kappa_f}\frac{1}{P_r}\frac{\partial^2 T}{\partial Y^2} \tag{10}$$

The initial and boundary conditions in non-dimensional quantities are given by

$$t \le 0 : U = 0, \; V = 0, \; T = 0 \text{ for all X and } Y$$
$$t > 0 : U = 1, \; V = 0, \; T = 1 \text{ at } Y = 0$$
$$U = 0, T = 0 \text{ at } X = 0$$
$$U \to 0, T \to 0 \text{ as } Y \to \infty \tag{11}$$

Let $E_1 = \frac{1}{(1-\phi)^{2.5}}\frac{1}{\left(1-\phi+\phi\frac{\rho_s}{\rho_f}\right)}$,

$$E_2 = \frac{\left(1-\phi+\phi\frac{(\rho\beta)_s}{(\rho\beta)_f}\right)}{\left(1-\phi+\phi\frac{\rho_s}{\rho_f}\right)}, \; E_3 = \frac{1}{\left(1-\phi+\phi\frac{\rho_s}{\rho_f}\right)},$$

$$E_4 = \frac{\kappa_{nf}}{\kappa_f}\frac{1}{\left(1-\phi+\phi\frac{(\rho C_p)_s}{(\rho C_p)_f}\right)}$$

$$, \; E_5 = \frac{1}{\left(1-\phi+\phi\frac{(\rho C_p)_s}{(\rho C_p)_f}\right)} \tag{12}$$

Now equations (9) and (10) in terms of E_1, E_2, E_3, E_4 and E_5 are

$$\frac{\partial U}{\partial t} + U\frac{\partial U}{\partial X} + V\frac{\partial U}{\partial Y} = E_1\frac{\partial^2 U}{\partial Y^2} + E_2 GrT - E_3 MU \tag{13}$$

$$\frac{\partial T}{\partial t} + U\frac{\partial T}{\partial X} + V\frac{\partial T}{\partial Y} = E_4\frac{1}{P_r}\frac{\partial^2 T}{\partial Y^2} \tag{14}$$

The analytical solution of Eq. (14) in the absence of inertial terms, subject to the boundary conditions (11) by using Laplace transform method is given by

$$T = erfc\left(\frac{y\sqrt{\mathrm{Pr}}}{2\sqrt{E_4 t}}\right) \tag{15}$$

3. NUMERICAL TECHNIQUE

An implicit finite difference scheme of Crank–Nicolson type has been used to solve the governing non-dimensional equations (8), (13) and (14) under the initial and boundary conditions (11). The finite difference equations corresponding to Equations (8), (13) and (14) are as follows:

$$\left[\frac{\begin{array}{l}U_{i,j}^{n+1} - U_{i-1,j}^{n+1} + U_{i,j}^{n} - U_{i-1,j}^{n} \\ +U_{i,j-1}^{n+1} - U_{i-1,j-1}^{n+1} + U_{i,j-1}^{n} - U_{i-1,j-1}^{n}\end{array}}{4\Delta X}\right] + \left[\frac{V_{i,j}^{n+1} - V_{i,j-1}^{n+1} + V_{i,j}^{n} - V_{i,j-1}^{n}}{2\Delta Y}\right] = 0 \tag{16}$$

$$\left[\frac{U_{i,j}^{n+1} - U_{i,j}^{n}}{\Delta t}\right] + U_{i,j}^{n}\left[\frac{\begin{array}{l}U_{i,j}^{n+1} - U_{i-1,j}^{n+1} \\ +U_{i,j}^{n} - U_{i-1,j}^{n}\end{array}}{2\Delta X}\right] + V_{i,j}^{n}\left[\frac{U_{i,j+1}^{n+1} - U_{i,j-1}^{n+1} + U_{i,j+1}^{n} - U_{i,j-1}^{n}}{4\Delta Y}\right] = E_1\left[\frac{\begin{array}{l}U_{i,j-1}^{n+1} - 2U_{i,j}^{n+1} + U_{i,j+1}^{n+1} \\ +U_{i,j-1}^{n} - 2U_{i,j}^{n} + U_{i,j+1}^{n}\end{array}}{2(\Delta Y)^2}\right] + \frac{G_r E_2}{2}\left[T_{i,j}^{n+1} + T_{i,j}^{n}\right] - \frac{ME_3}{2}\left[U_{i,j}^{n+1} + U_{i,j}^{n}\right] \tag{17}$$

$$\left[\frac{T_{i,j}^{n+1}-T_{i,j}^{n}}{\Delta t}\right]+U_{i,j}^{n}\left[\frac{\begin{array}{c}T_{i,j}^{n+1}-T_{i-1,j}^{n+1}\\ +T_{i,j}^{n}-T_{i-1,j}^{n}\end{array}}{2\Delta X}\right]$$

$$+V_{i,j}^{n}\left[\frac{T_{i,j+1}^{n+1}-T_{i,j-1}^{n+1}+T_{i,j+1}^{n}-T_{i,j-1}^{n}}{4\Delta Y}\right] \qquad (18)$$

$$=\frac{E_4}{\mathrm{P}_r}\left[\frac{\begin{array}{c}T_{i,j-1}^{n+1}-2T_{i,j}^{n+1}+T_{i,j+1}^{n+1}\\ +T_{i,j-1}^{n}-2T_{i,j}^{n}+T_{i,j+1}^{n}\end{array}}{2(\Delta Y)^2}\right]$$

The method of solving the above finite difference equations using Crank–Nicolson type has been discussed by Ramachandra Prasad *et al*. (2007). The region of integration is considered as a rectangle with sides $X=0$ to $X_{\max}=1$ and $Y=0$ to $Y_{\max}=14$, where $Y_{\max}$ corresponds to $Y=\infty$ which lies very well outside the momentum and energy boundary layers. After experimenting with a few sets of mesh sizes to access grid independence, the time and spatial step sizes $\Delta t=0.01$, $\Delta X=0.05$ and $\Delta Y=0.25$ were found to give accurate results. The Crank–Nicolson implicit finite difference scheme is always stable and convergent. To check the accuracy of the numerical results, the temperature profiles of the present study are compared with the analytical solution given by equation (15) in Figure 2 and found to be in very good agreement. Confidence in the implicit finite-difference numerical solutions is therefore high.

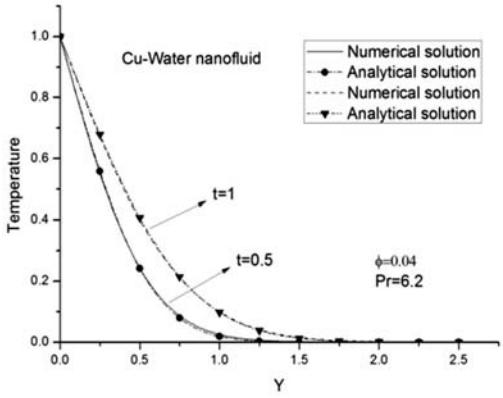

Fig. 2. Comparison of temperature profiles.

4. RESULTS AND DISCUSSION

In order to get a physical insight into the problem, a representative set of numerical results is shown graphically in Figs. 3-8, to illustrate the influence of significant parameters such as nanoparticle volume fraction, magnetic parameter thermal Grashof number and time on the velocity and the temperature profiles in the boundary layer region. Four different types of nanofluids containing aluminium oxide (Al_2O_3), copper (Cu), titanium oxide (TiO_2) and silver (Ag) nanoparticles with water as a base fluid are considered. The nanoparticle volume fraction is considered in the range of $0\le\phi\le 0.04$, as sedimentation takes place when the nanoparticle volume fraction exceeds 8%. In this study, Spherical nanoparticles with thermal conductivity and dynamic viscosity shown in Model I in Table 2(see Hamilton RL and Crosser *OK* (1962), Loganathan *et al*. (2013)) are considered. The Prandtl number, *Pr* of the base fluid is kept constant at 6.2.When φ = 0 this study reduces the governing equations to those of a regular fluid i.e. nanoscale characteristics are eliminated.

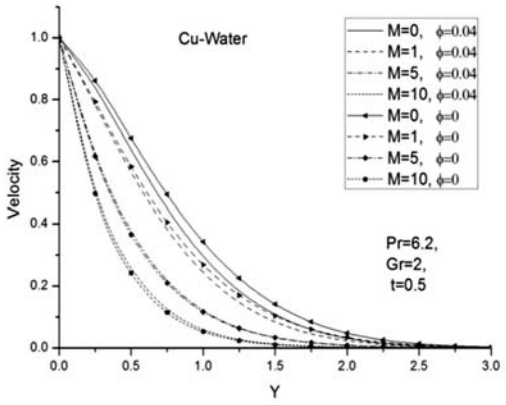

Fig. 3. Effect of Magnetic parameter M on the velocity profiles.

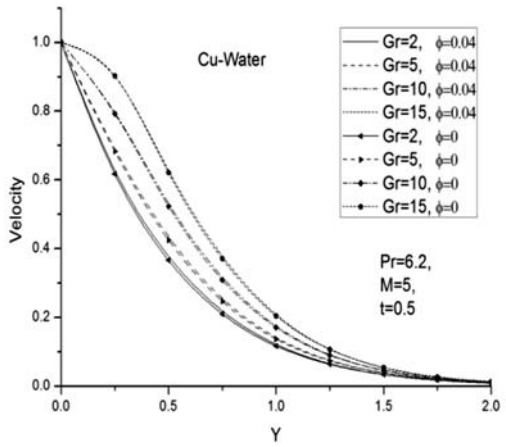

Fig. 4. Effect of thermal Grashof number Gr on the velocity profiles.

The transient velocity and temperature profiles of *Cu* -water nanofluid and pure water ($\phi=0$)with coordinate Y for different values of magnetic parameter M and nanoparticle volume fraction ϕ are shown in Figures 3 and 6 respectively. It is observed in figure 3 that, the flow rate of *Cu* -water nanofluid retards and thereby giving rise to a decrease in the velocity profiles with the increase in magnetic parameter M. The reason behind this phenomenon is that application of magnetic field to

an electrically conducting nanofluid gives rise to a resistive type force called the Lorentz force. This force has the tendency to slow down the motion of the nanofluid in the boundary layer. But in Figure 6, the temperature of the Cu -water nanofluid is found to increase with the increase in M. This implies that the thermal boundary layer thickness increases with the increase in M. Also, it is found in Figure 3 that, in the absence of the magnetic field (when M=0) or in the presence of small magnetic parameter (when M=1), the velocity of the Cu -water nanofluid decreases with the increase in nanoparticle volume fraction ϕ. But, in the presence of large magnetic parameters (when M=5, 10), the reverse effect of the nanoparticle volume fraction ϕ is noticed on the velocity of Cu -water nanofluid. Furthermore, it is found in Figure 6 that, in the presence or in the absence of magnetic field, the temperature of the Cu -water nanofluid increases with the increase in nanoparticle volume fraction ϕ. Thus, the thermal boundary layer thickness increases with a rise in the values of ϕ in the presence or absence of the magnetic field.

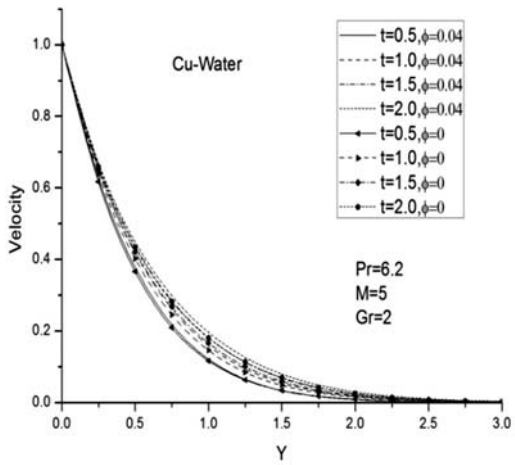

Fig. 5. Effect of time t on the velocity profiles.

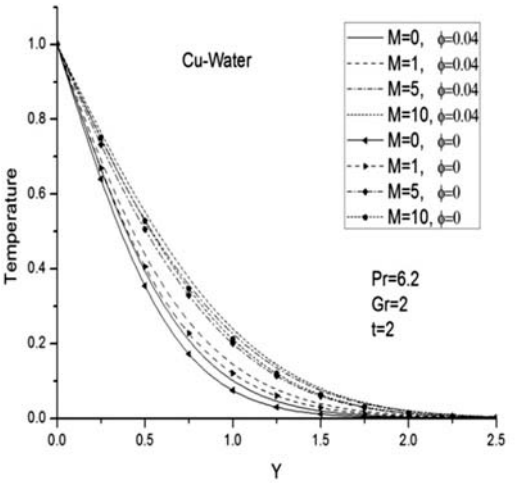

Fig. 6. Effect of Magnetic parameter M on the temperature profiles.

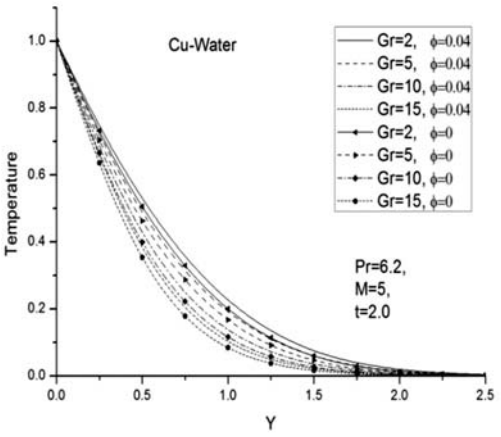

Fig. 7. Effect of thermal Grashof number Gr on the temperature profiles.

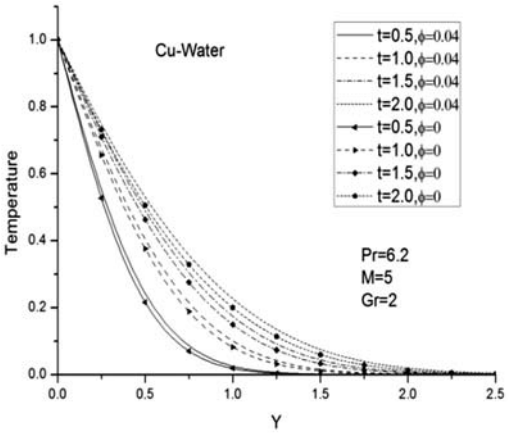

Fig. 8. Effect of time t on the temperature profiles.

The effects of thermal Grashof number Gr and nanoparticle volume fraction ϕ on the transient velocity and temperature profiles of Cu -water nanofluid and pure water ($\phi = 0$) with coordinate Y are shown in Figures 4 and 7 respectively. The parameter $G_r = \dfrac{g\beta_f \nu_f \left(T_w' - T_\infty'\right)}{u_0^3}$ denotes the relative influence of thermal buoyancy force and viscous force in the boundary layer regime. With large values of this parameter, buoyancy dominates and for small values viscosity dominates. In Figure 4, the velocity of Cu -water nanofluid is found to increase with the increase in thermal Grashof number Gr. This means that the buoyancy force accelerates velocity field. An increase in the value of thermal Grashof number has the tendency to induce much flow in the boundary layer due to the effect of thermal buoyancy. But it is found in Figure 7 that, the temperature of Cu -water nanofluid decreases with the increase in thermal Grashof number Gr. This means that buoyancy force reduces temperature field. Furthermore, it is observed in the Figures that, the velocity and temperature of the Cu -Water nanofluid is more than that for pure

water (Newtonian viscous fluid) for all values of thermal Grashof number Gr.

The development of transient velocity and temperature profiles of *Cu* -water nanofluid and pure water ($\phi = 0$) for different values of time twith coordinate Y is shown in Figures 5 and 8 respectively. In Figures the velocity and temperature profiles of *Cu* -water nanofluid are found to increase with a rise in time. It is also found in the Figures that, the velocity and temperature of the *Cu* -water nanofluid increases with the increase in nanoparticles volume fraction ϕ for all values of t (time). Furthermore the velocity and temperature profiles of *Cu* -water nanofluid are found to decrease monotonically from the value unity at the surface of the plate to zero along the coordinate Y for all values of M (magnetic parameter), Gr (thermal Grashof number), t (time) and ϕ (nanoparticle volume fraction), which is evident in Figures 3-8.

In materials processing problems, characteristics at the wall are important, for example the skin friction coefficient C_f and the Nusselt number Nu, which are defined, respectively, as follows:

$$C_f = \frac{\tau_w}{\rho_f u_0^2}, \qquad Nu = \frac{q_w L_{ref}}{\kappa_f (T_w' - T_\infty')} \tag{19}$$

Where τ_w is the skin-friction or shear stress and q_w is the heat flux or the rate of heat transfer from the surface of the plate, and they are given by

$$\tau_w = \mu_{nf} \left(\frac{\partial u}{\partial y} \right)_{y=0}, q_w = -\kappa_{nf} \left(\frac{\partial T'}{\partial y} \right)_{y=0} \tag{20}$$

Using non-dimensional variables (7), we get

The skin friction coefficient

$$C_f = \frac{1}{(1-\phi)^{2.5}} \left(\frac{\partial U}{\partial Y} \right)_{Y=0} \tag{21}$$

and The Nusselt number $Nu = -\frac{\kappa_{nf}}{\kappa_f} \left(\frac{\partial T}{\partial Y} \right)_{Y=0}$

(22)

The derivatives involved in Equations (21) and (22) are evaluated using five-point approximation formula.

The effects of different values of nanoparticle volume fraction ϕ for different types of nanofluids namely, aluminium oxide, copper, titanium oxide and silver on the skin friction coefficient and the Nusselt number are shown in Tables 3 and 8 respectively. It is seen in Tables 3 and 8 that, the skin-friction coefficient decreases and the Nusselt number increases at the surface with the increase in nanoparticle volume fraction for all nanofluids namely, aluminium oxide, copper, titanium oxide and silver. It is also seen in table 3 that, Al_2O_3 -Water nanofluid attains the maximum value of the skin friction coefficient relative to the other nanofluids for all values of ϕ.But it is found in table 8 that, the values of the Nusselt number decrease from *Cu* -Water nanofluid to TiO_2 -water nanofluid through Al_2O_3 and *Ag* -water nanofluids. This confirms that *Cu* -Water nanofluid attains an enhanced heat transfer rate when compared with the other nanofluids for all values of ϕ.

Table 3 Effects of the nanoparticle volume fraction for different types of nanofluids on skin friction coefficient when Pr=6.2, M=5, Gr=2, X=1, t=0.5

ϕ	Nanoparticles			
	Ag	*Cu*	TiO_2	Al_2O_3
0	-1.8499	-1.8499	-1.8499	-1.8499
0.01	-1.8784	-1.8786	-1.8781	-1.8775
0.02	-1.9083	-1.9084	-1.9070	-1.9059
0.03	-1.9395	-1.9394	-1.9368	-1.9351
0.04	-1.9721	-1.9716	-1.9674	-1.9651

Table 4 Effects of the magnetic parameter for different types of nanofluids on skin friction coefficient when Pr=6.2, Gr=2, ϕ=0.04, X=1, t=0.5

M	Nanoparticles			
	Ag	*Cu*	TiO_2	Al_2O_3
0	-0.5464	-0.5258	-0.4550	-0.4476
1	-0.8976	-0.8844	-0.8391	-0.8336
5	-1.9721	-1.9716	-1.9674	-1.9651
10	-2.8816	-2.8842	-2.8889	-2.8875

Table 5 Effects of the thermal Grashof number for different types of nanofluids on skin friction coefficient when Pr=6.2, M=5, ϕ=0.04, X=1, t=0.5

Gr	Nanoparticles			
	Ag	*Cu*	TiO_2	Al_2O_3
2	-1.9721	-1.9716	-1.9674	-1.9651
5	-1.4217	-1.4260	-1.4299	-1.4249
10	-0.5045	-0.5167	-0.5340	-0.5246
15	0.4127	0.3925	0.3618	0.3757

Table 6 Effects of the time for different types of nanofluids on skin friction coefficient when Pr=6.2, M=5, ϕ=0.04, X=1, Gr=2

t	Nanoparticles			
	Ag	*Cu*	TiO_2	Al_2O_3
0.2	-2.3320	-2.3144	-2.2610	-2.2560
0.5	-1.9721	-1.9716	-1.9674	-1.9651
0.8	-1.8757	-1.8789	-1.8846	-1.8828
1.0	-1.8393	-1.8435	-1.8516	-1.8500

Table 7 Effects of the Coordinate X for different types of nanofluids on skin friction coefficient when Pr=6.2, M=5, ϕ=0.04, t=0.5, Gr=2

X	Nanoparticles			
	Ag	Cu	TiO_2	Al_2O_3
0.2	-2.2969	-2.2836	-2.2418	-2.2369
0.5	-1.9811	-1.9803	-1.9752	-1.9728
0.8	-1.9721	-1.9716	-1.9675	-1.9652
1.0	-1.9721	-1.9716	-1.9674	-1.9651

Table 8 Effects of the nanoparticle volume fraction for different types of nanofluids on Nusselt number when Pr=6.2, M=5, Gr=2, X=1, t=1.0

ϕ	Nanoparticles			
	Cu	Ag	Al_2O_3	TiO_2
0	1.4280	1.4280	1.4280	1.4280
0.01	1.4468	1.4450	1.4452	1.4423
0.02	1.4657	1.4621	1.4626	1.4566
0.03	1.4848	1.4794	1.4801	1.4711
0.04	1.5041	1.4967	1.4977	1.4856

Table 9 Effects of the magnetic parameter for different types of nanofluids on Nusselt number when Pr=6.2, ϕ=0.04, Gr=2, X=1, t=1.0

M	Nanoparticles			
	Cu	Ag	Al_2O_3	TiO_2
0	1.5646	1.5546	1.5657	1.5531
1	1.5383	1.5297	1.5350	1.5228
5	1.5041	1.4967	1.4977	1.4856
10	1.4994	1.4921	1.4930	1.4809

Table 10 Effects of the thermal Grashof number for different types of nanofluids on Nusselt number when Pr=6.2, ϕ=0.04, M=5, X=1, t=1.0

Gr	Nanoparticles			
	Cu	Ag	Al_2O_3	TiO_2
2	1.5041	1.4967	1.4977	1.4856
5	1.5151	1.5076	1.5086	1.4964
10	1.5551	1.5477	1.5484	1.5359
15	1.6211	1.6138	1.6140	1.6007

Table 11 Effects of the time for different types of nanofluids on Nusselt number when Pr=6.2, ϕ =0.04, M=5, Gr=2, X=1

t	Nanoparticles			
	Cu	Ag	Al_2O_3	TiO_2
0.2	4.0349	4.0117	4.0181	3.9905
0.5	2.2147	2.2020	2.2054	2.1904
0.8	1.6887	1.6801	1.6816	1.6684
1.0	1.5041	1.4967	1.4977	1.4856

Table 12 Effects of the Coordinate X for different types of nanofluids on Nusselt number when Pr=6.2, ϕ=0.04, M=5, Gr=2,t=1

X	Nanoparticles			
	Cu	Ag	Al_2O_3	TiO_2
0.2	3.9565	3.9154	3.9903	3.9646
0.5	1.9760	1.9619	1.9718	1.9604
0.8	1.5469	1.5389	1.5402	1.5285
1.0	1.5041	1.4967	1.4977	1.4856

The effects of different values of magnetic parameter on the skin friction coefficient and the Nusselt number for various types of nanofluids namely, aluminium oxide, copper, titanium oxide and silver are presented in Tables 4 and 9. The skin-friction coefficient and the Nusselt number at the surface are found to decrease for all nanofluids namely aluminium oxide, copper, titanium oxide and silver with increase in magnetic parameter. It is seen in table 4 that, in the absence or presence of magnetic field (when M=0, 1, 5) skin friction coefficient magnitudes decrease from the Ag-Water nanofluid to Al_2O_3-water through Cu and TiO_2-water nanofluids. This proves that Ag-Water nanofluid achieves maximum skin friction coefficient at surface in magnitude comparative to the other nanofluids. But, when M=10, TiO_2-Water nanofluid attains the maximum skin friction coefficient in magnitude relative to the other nanofluids. However it is seen in table 9 that, in the presence of magnetic field (when M=1, 5, 10), the values of the Nusselt number decreases from Cu-Water nanofluid to TiO_2-water nanofluid through Al_2O_3, and Ag-water nanofluids. This shows that Cu-Water nanofluid attains an improved heat transfer rate when compared with the other nanofluids in the presence of magnetic field for all values of M. But in the absence of magnetic field (when M=0), the values of the Nusselt number decreases from Al_2O_3-Water nanofluid to TiO_2-water nanofluid through Cu, and Ag-water nanofluids. This confirms that Al_2O_3-Water nanofluid gets a better heat transfer rate when compared with the other nanofluids in the absence magnetic field.

Tables 5 and 10 show the effects of different values of thermal Grashof number on the skin friction coefficient and the Nusselt number for different types of nanofluids namely aluminium oxide, copper, titanium oxide and silver. It is seen in Tables 5 and 10 that, an increase in the thermal Grashof number enhance the skin-friction coefficient and also the Nusselt number at the surface for all nanofluids namely, aluminium oxide, copper, titanium oxide and silver. It is also seen in table 5 that, in the presence of thermal Grashof number (when Gr=5, 10, 15) Skin friction coefficient at surface for Ag-Water achieves the

maximum relative to the other nanofluids. But when Gr=2, Ag -Water nanofluid achieves the minimum skin friction coefficient at surface relative to the other nanofluids. But it is found in Table 10 that, the values of Nusseltnumber decrease from Cu -Water nanofluid to TiO_2 -water nanofluid through Al_2O_3 , and Ag -water nanofluids. This shows that Cu -Water nanofluid attains an enhanced heat transfer rate when compared with the other nanofluids for all values of Gr.

Tables 6 and 11show the effects of different values of time t on the skin friction coefficient and the Nusselt number for different types of nanofluids namely aluminium oxide, copper, titanium oxide and silver.It is seen in tables 6 and 11 that, as time progress, the skin-friction coefficient increase and the Nusselt number decrease at the surface for all nanofluids namely, aluminium oxide, copper, titanium oxide and silver.It is also seen in table 6 that, when time t=0.2, 0.5, Skin friction coefficient at surface for Ag -Water achieves the minimum, but when time t=0.8, 1.0, it attains the maximum at surface relative to the other nanofluids. However the values of Nusselt number are found to decrease from Cu -Water nanofluid to TiO_2 -water nanofluid through Al_2O_3 and Ag -water nanofluids. This shows that Cu -Water nanofluid attains an improved heat transfer rate when compared with the other nanofluids for all values of t, which is clear in Table 11.

The effects of different values of coordinate X, for different types of nanofluids namely aluminium oxide, copper, titanium oxide and silver, on the skin friction coefficient and the Nusselt number are presented in Tables 7 and 12.It is observed in tables 7 and 12 that, the skin-friction coefficient at the surface increases and the Nusselt number decreases for all nanofluids namely, aluminium oxide, copper, titanium oxide and silver with the increase in X coordinate.It is also observed in table 7 that, Ag -Water nanofluid achieves the maximum Skin friction coefficient in magnitude, while Al_2O_3 -Water nanofluidattains the minimumin magnitude relative to the other nanofluids for all values of X coordinate.Furthermore it is noticed in table 12 that, when X=0.5, 0.8, 1, the values of Nusselt number decreases from Cu -Water nanofluid to TiO_2 -water nanofluid through Al_2O_3 , and Ag -water nanofluids. This shows that Cu -Water nanofluid attains an improved heat transfer rate when compared with the other nanofluids for all X=0.5, 0.8, 1. But when X=0.2, the values of Nusselt number decreases from Al_2O_3 -Water nanofluid to Ag -water nanofluid through TiO_2 , and Cu -water nanofluids. This proves that Al_2O_3 -Water nanofluid achieves an enhanced heat transfer rate when compared with the other nanofluids for X=0.2.

5 CONCLUSIONS

In this paper, the problem of transient free convection flow and heat transfer of nanofluid past an impulsively started semi-infinite vertical plate in the presence of magnetic field has been investigated. An implicit finite difference scheme of Crank–Nicolson type has been used to solve the governing non-dimensional equations with the corresponding initial and boundary conditions.The effects of significant parameters such as nanoparticle volume fraction, magnetic parameter, thermal Grashof number, time and nanofluids type on the flow and heat transfer characteristics have been discussed.

The conclusions of the study are as follows:

1) As the nanoparticle volume fraction increased, the skin-friction coefficient decreased and the Nusselt number increased at the surface for all nanofluids namely, aluminium oxide, copper, titanium oxide and silver.

2) As the magnetic parameter increased, the skin-friction coefficient and the Nusselt number at the surface decreased for all nanofluids aluminium oxide, copper, titanium oxide and silver.

3) As the thermal Grashof number increased, the skin-friction coefficient and the Nusselt number at the surface increased for all nanofluids namely, aluminium oxide, copper, titanium oxide and silver.

4) As time progressed, the skin-friction coefficient at the surface increased and the Nusselt number decreased for all nanofluids namely, aluminium oxide, copper, titanium oxide and silver.

5) The skin-friction coefficient at the surface increased and The Nusselt number decreased for all nanofluids namely, aluminium oxide, copper, titanium oxide and silver with the increase in X coordinate.

6) Selecting Al_2O_3 as the nanoparticle leads to the maximum value of the skin friction coefficient for all values of ϕ .

7) Choosing copper as the nanoparticle leads to the maximum amount of Nusselt number for all values of ϕ .

8) In the presence of magnetic field, Cu -Water nanofluid attained an improved heat transfer rate when compared with the other nanofluids for all values of M.

9) In the absence magnetic field Al_2O_3 -Water nanofluid achieved an enhanced heat transfer rate when compared with the other nanofluids.

10) Cu -Water nanofluid attained an improved heat transfer rate when compared with the other nanofluids for all values of Gr.

11) *Cu* -Water nanofluid achieved an improved heat transfer rate when compared with the other nanofluids for all values of t.

ACKNOWLEDGEMENTS

The authors are grateful to the Editors and Reviewers of this journal, for their constructive comments which have helped to improve the present article.

REFERENCES

Abu-Nada, E. and H. F. Oztop (2009). Effects of inclination angle on natural convection in enclosures filled with Cu-water nanofluid. *Int J Heat Fluid Flow* 30, 669–678.

Abu-Nada, E., F. O. Hakan and I. Pop (2012). Buoyancy induced flow in a nanofluid filled enclosure partially exposed to forced convection. *Superlattices and Microstructures* 51, 381–395.

Akbarinia, A., M. Abdolzadeh and R. Laur (2011). Critical investigation of heat transfer enhancement using nanofluids in microchannels with slip and non-slip flow regimes. *Appl Therm Eng* 31, 556–565.

Anwar Bég, O., J. Zueco, S. K. Ghosh and A. Heidari (2011). Unsteady magneto hydrodynamic heat transfer in a semi-infinite porous medium with thermal radiation flux: analytical and numerical study. *Advances in Numerical Analysis,* 1-17.

Chamkha, A. J., A. M. Aly and H. Al-Mudhaf (2010a). Laminar MHD mixed convection flow of a nanofluid along a stretching permeable surface in the presence of heat generation or absorption effects. *Int J Microscale Nanoscale Therm Fluid Transp Phenom* (in press)

Chamkha, A. J., A. M. Rashad and E. Al-Meshaiei (2011). Melting effect on unsteady hydromagnetic flow of a nanofluid past a stretching sheet. *Int J Chem React Eng* 9, 1–23.

Chamkha, A. J., R. S. R. Gorla and K. Ghodeswar (2010b). Nonsimilar solution for natural convective boundary layer flow over a sphere embedded in a porous medium saturated with a nanofluid. *Transp Porous Media* 86, 13–22.

Chamkha, A. J., S. Abbasbandy, A. M. Rashad and K. Vajravelu (2012). Radiation effects on mixed convection over a wedge embedded in a porous medium filled with a nanofluid. *Transp Porous Media* 91, 261–279.

Chen, J., S. K. Tyagi, S. C. Kaushik, V. Tiwari and C. Wu (2005). Effects of several major irreversibilities on the thermodynamic performance of a regenerative MHD power cycle.*ASME J. Energy Resour. Technol.* 127(2), 103-118.

Choi, S. U. S. (1995). Enhancing Thermal Conductivity of Fluids with Nanoparticles. *Developments and Applications of Non-Newtonian Flows* FED-231/MDvol. 66, 99–105.

Choi, S. U. S. (2009). Nanofluids: from vision to reality through research. *J of Heat Transf* 131, 1–9.

Das, M., B. K. Mahatha, R. Nandkeolyar, B. K. Mandal and K. Saurabh (2014). Unsteady Hydromagnetic Flow of a Heat Absorbing Dusty Fluid Past a Permeable Vertical Plate with Ramped Temperature.*Journal of Applied Fluid Mechanics*7(3), 485-492.

Duangthongsuk, W. and S. Wongwises (2008). Effect of thermophysical properties models on the predicting of the convective heat transfer coefficient for low concentration nanofluid. *Int Commun Heat Mass Transf* 35, 1320–1326.

ELKabeir, S. M. M., M. Modather and A. M. Rashad (2015). Heat and Mass Transfer by Unsteady Natural Convection over a Moving Vertical Plate Embedded in a Saturated Porous Medium with Chemical Reaction, Soret and Dufour Effects. *Journal of Applied Fluid Mechanics* 8(3), 453-463.

Gangadhar, K. (2015). Radiation, Heat Generation and Viscous Dissipation Effects on MHD Boundary Layer Flow for the Blasius and Sakiadis Flows with a Convective Surface Boundary Condition. *Journal of Applied Fluid Mechanics* 8(3), 559-570.

Gorla, R. S. R., Chamkha Ali J. and A. M. Rashad (2011b). Mixed convective boundary layer flow over a vertical wedge embedded in a porous medium saturated with a nanofluid. *J Nanoscale Res Lett* 6, 207.

Gorla, R. S. R., S. M. M. EL-Kabeir and A. M. Rashad (2011a). Heat transfer in the boundary layer on a stretching circular cylinder in a nanofluid. *J Thermophys Heat Transf* 25, 183–186.

Hamilton, R. L. and O. K. Crosser (1962). Thermal conductivity of Heterogeneous two component system. *Ind &Eng Chem. Fundamentals* 1, 187-191.

Ibrahim, W. and B. Shanker (2014). Magnetohydrodynamic boundary layer flow and heat Transfer of a nanofluid over non-isothermal stretching sheet.*ASME J. Heat Transfer* 136(5), 051701-051701-9.

Loganathan, P., P. Nirmal chand and P. Ganesan (2013). Radiation effects on an unsteady natural convective flow of a nanofluid past an infinite vertical plate. *NANO: Brief Reports and Reviews* 8(1), 1-10.

Mukhopadhyay, S. (2011). Heat transfer analysis for unsteady MHD flow past a non-isothermal stretching surface. *Nuclear Engineering and Design* 241(12), 4835-4839.

Murshed, S. M. S. (2011). A review of boiling and convective heat transfer with nanofluids. *Renewable and Sustainable Energy Reviews* 15, 2342–2354.

Nield, D. A. and A. V. Kuznetsov (2009). The Cheng-Minkowycz problem for natural convective boundary-layer flow in a porous medium saturated by a nanofluid. *Int J Heat Mass Transf* 52, 5792–5795.

Oztop, H. F. and E. Abu-Nada (2008). Numerical study of natural convection in partially heated rectangular enclosures filled with nanofluids. *Int. J. Heat Fluid flow* 29, 1326-1336.

Rajesh, V. and O. Anwar Beg (2014). MHD transient nanofluid flow and heat transfer from a moving vertical cylinder with temperature oscillation. *Computational Thermal Sciences* 6(5), 439-450.

Rajesh, V., A. J. Chamkha and M. P. Mallesh (2016). Nanofluid flow past an impulsively started vertical plate with variable surface temperature. *International Journal of Numerical Methods for Heat & Fluid Flow* (in press).

Rajesh, V., O. Anwar Beg and M. P. Mallesh (2014). Transient nanofluid flow and heat transfer from a moving vertical cylinder in the presence of thermal radiation: Numerical study. *Proc IMechE Part N: J Nanoengineering and Nanosystems*. OnlineFirst, published September 5.

Ramachandra Prasad, V., N. Bhaskar Reddy and R. Muthucumaraswamy (2007). Radiation and mass transfer effects on two-dimensional flow past an impulsively started infinite vertical plate. *International Journal of Thermal Science* 46, 1251-1258.

Rashad, A. M., M. A. EL-Hakiem and Abdou M. M. M. (2011). Natural convection boundary layer of a non-Newtonian fluid about a permeable vertical cone embedded in a porous medium saturated with a nanofluid. *Comput Math Appl.* 62, 3140–3151.

Seth, G. S., R. Sharma and S. Sarkar (2015). Natural Convection Heat and Mass Transfer Flow with Hall Current, Rotation, Radiation and Heat Absorption Past an Accelerated Moving Vertical Plate with Ramped Temperature. *Journal of Applied Fluid Mechanics* 8(1), 7-20.

Tiwari, R. K. and M. K. Das (2007). Heat transfer augmentation in a two-sided lid-driven differentially heated square cavity utilizing nanofluids. *Int. J. Heat and Mass Transf.* 50(9-10), 2002-2018.

Turkyilmazoglu, M. (2014). unsteady convection flow of some nanofluids past a moving vertical flat plate with heat transfer. *ASME Journal of Heat Transfer* 136, 1-7.

Turkyilmazoglu, M. and I. Pop (2013). Heat and mass transfer of unsteady natural convection flow of some nanofluids past a vertical infinite flat plate with radiation effect. *International Journal of Heat and Mass Transfer* 59, 167–171.

Yamaguchi, H., X. D. Niu and X. R. Zhang (2011). Investigation on a low-melting-point gallium alloy MHD power generator. *Int. J. Energy Research* 35(10), 209–220.

Yu, W., D. M. France, J. L. Routbort and U. S. Choi (2008). Review and comparison of nanofluid thermal conductivity and heat transfer enhancements. *Heat Transfer Engineering* 29(5), 432–460.